04,08

Zinc tungstate: luminescence and magnetic resonance

© M.Yu. Artyomov[1], V.A. Vazhenin[1], A.P. Potapov[1], K.A. Soubbotin[2,3], Yu.I. Zimina[2,3], A.V. Fokin[1], A.V. Popov[3,4], O.N. Lis[2]

[1] Ural Federal University (Institute of Natural Sciences and Mathematics), Yekaterinburg, Russia
[2] Prokhorov Institute of General Physics, Russian Academy of Sciences, Moscow, Russia
[3] Mendeleev University of Chemical Technology, Moscow, Russia
[4] Institution of the Russian Academy of Sciences Institute for Theoretical and applied electromagnetics RAS, Moscow, Russia

E-mail: Vladimir.Vazhenin@urfu.ru

Received November 25, 2025
Revised November 25, 2025
Accepted November 27, 2025

Significant differences in the luminescence decay kinetics of thulium ions were observed in different parts of a zinc tungstate single crystal doped with thulium and lithium. EPR studies of uncontrolled Fe^{3+}, Cr^{3+}, and Gd^{3+} impurity ions were performed on four parts of this crystal to determine their concentrations and the degree of association of Gd^{3+}-V_{Zn} and Gd^{3+}-Li_{Zn} centers, which may correlate with optical properties.

Keywords: zinc tungstate, impurity ions, luminescence, paramagnetic resonance.

DOI: 10.61011/PSS.2026.01.63239.332-25

1. Introduction

The Tm:$ZnWO_4$ crystal is a promising active medium for two-micron solid-state lasers operating at the $^3F_4 \rightarrow {}^3H_6$ transition. Lasers of this range are widely used in laser surgery [1], remote sensing of the atmosphere [2] as pumping sources for mid-infrared lasers [3,4] and many other fields. The Tm:$ZnWO_4$ crystal as the active medium of such lasers has a number of advantages, including:

– significant inhomogeneous broadening of the emission and absorption bands of Tm^{3+} ions [5,6], convenient for diode pumping of lasers and for obtaining ultrashort pulses under mode-locked operation;

– significant Stark splitting of the ground state $^3H_6$ of Tm^{3+} ions, which leads to a decrease in the generation threshold due to a very weak spectral overlap of the radiation band at the transition $^3F_4 \rightarrow {}^3H_6$ and absorption at the reverse transition [2,3,7,8], which allows thulium laser generation at the specified transition at wavelengths exceeding $2\,\mu$m [5];

– high values and strong anisotropy of peak absorption cross sections and stimulated luminescence [5,6], which is a necessary condition for obtaining intense and linearly polarized laser radiation.

In addition, $ZnWO_4$ crystals have good thermal conductivity [9] and can be grown by the Czochralski method [3,10]. At the same time, optimization of the type (ions Li^+) and the charge concentration of the charge compensator of the heterovalent substitution $Zn^{2+} \rightarrow Tm^{3+}$ made it possible to bring the distribution coefficient of the activator between the crystal and the melt to a fairly decent value of 0.45, and the available actual concentrations of the activator in the crystal — up to several at.% (hereinafter — relative to Zn^{2+}) while maintaining acceptable optical quality and mechanical strength characteristics of the samples [6].

As is known, in the scheme of operation of two-micron thulium lasers at the above spectral transition with semiconductor diode pumping at the $^3H_4$ level, the cross-relaxation process plays a key role ($^3H_4 \rightarrow {}^3F_4$; $^3H_6 \rightarrow {}^3F_4$). When this process proceeds efficiently, the quantum yield of optical pumping and generation of two-micron thulium lasers significantly exceeds 100 %. The most important and informative tool for studying this process is the measurement and analysis of the kinetics of luminescence attenuation of thulium ions from the $^3H_4$ level at different concentrations of the activator in the same matrix.

Studying the kinetics of attenuation of this luminescence in a series of Tm, Li:$ZnWO_4$ crystals with different combinations of concentrations of doping impurities, we found a special behavior of the kinetics measured in different areas of the same sample (see Figure 1) grown from a melt with nominal concentrations of Tm and Li of 4 at.% each (hereinafter referred to as — 4 % Tm + 4 % Li).

At the final stage of kinetics (after $40\,\mu$s after Δ-pulse excitation and beyond), the luminescence attenuation curves for all sections of the crystal are monoexponential and differ rather weakly from each other (approximation of these sections by a monoexponential function shows the lifetimes of $132\,\mu$s, $126\,\mu$s and $120\,\mu$s for the initial, middle and final sections of the sample, respectively). These differences can easily be explained by a gradual increase in thulium

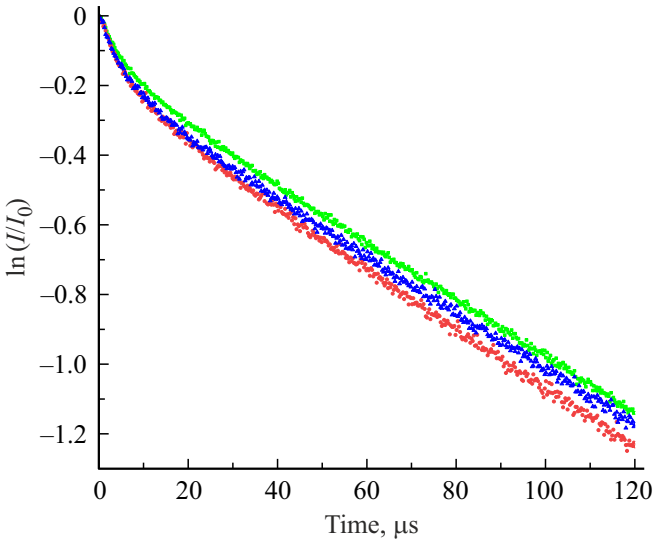

Figure 1. Kinetics of thulium ion luminescence attenuation from the $^3H_4$ level at various sites of the sample 4 % Tm + 4 % Li (beginning — blue dots, middle — green, end — red). Excitation wavelength — 808 nm, monitoring wavelength — 825 nm, temperature — 300 K.

concentration along the length of the sample due to the not very high thulium distribution coefficient between the crystal and the melt in this sample [6]. Indeed, a study of the polarized optical absorption spectra of the specified parts of this sample at 300 K revealed a slight monotonous increase in the concentration of Tm^{3+} ions from the beginning to the end of the boule from 0.92 ± 0.08 to 0.99 ± 0.03 at.% relative to zinc.

At the same time, the initial stages of luminescence attenuation kinetics of this sample (no more than 40 μs after Δ-pulsed excitation) have an abnormally high decay rate. Moreover, the type of this kinetic stage for the middle part of the sample differs markedly from that for the initial and final parts. This may indicate that there are serious differences in different parts of this crystal:

– concentrations of thulium ion associates with each other;

– concentrations of uncontrolled trace elements actively involved in luminescence suppression;

– center compositions of Tm^{3+} ions, i. e., by the presence, type and/or concentrations of point defects located in the nearest environment of these ions. Such defects introduce significant disturbances into the crystal field on thulium ions, which can affect the probabilities of radiative and nonradiative processes;

However, according to the results of this study, it can be stated that there is no fundamental difference in the concentration of lithium in different areas of the crystal, since earlier [6] it was found that the absorption spectra of Tm:$ZnWO_4$ crystals containing and not containing lithium differ markedly in the shape of the bands (according to the ratio of probabilities of individual Stark components of spectral transitions). No such differences were found in spectra taken at various sites of the crystal $ZnWO_4$: 4 % Tm + 4 % Li.

To further verify the various versions of the causes of the mentioned differences in the kinetics of luminescence attenuation, we carried out studies of various sections of the sample $ZnWO_4$: 4 % Tm/4 % Li using the electron paramagnetic resonance (EPR) method, which is known to be sensitive to differences in the immediate environment of paramagnetic (spectroscopically active) centers, as well as to microconcentrations of uncontrolled paramagnetic impurities, which can be centers of nonradiative relaxation of excited states of rare-earth activators in laser crystals.

In our work [11], the uncontrolled impurity centers Fe^{3+} (electron spin $S = 5/2$), Cr^{3+} ($S = 3/2$) and Gd^{3+} ($S = 7/2$) (the so-called Fe1, Cr1 and Gd1)were studied by the EPR method in a $ZnWO_4$ crystal doped with thulium only ($S = 3/2$) and Gd^{3+} ($S = 7/2$) (the so-called Fe1, Cr1 and Gd1), replacing Zn^{2+} ions and retained symmetry of the position C_2 [12–16]. Along with these monoclinic paramagnetic centers (PC), EPR spectra of triclinic centers (Fe2, Fe3, Cr2, Cr3) were observed, whose signals as satellites accompanied the Fe1, Cr1 transitions in a wide range of magnetic field orientations [17,18]. On the contrary, the triclinic centers Gd2, Gd3 had a very different orientation behavior from Gd1. Most likely, all these centers are caused by dimeric complexes of a paramagnetic ion with a close zinc vacancy. It should be noted that the triclinic centers with numbers 2 and 3 are connected by the operation C_2 of the crystal, and their spectra become equivalent at $\mathbf{B} \parallel \mathbf{b}$ and when $\mathbf{B}$ is in the plane $\mathbf{a}-\mathbf{c}$ ($\mathbf{B}$ — magnetic field induction vector).

We studied in Ref. [19] the EPR of uncontrolled impurity centers Fe^{3+}, Cr^{3+}, Gd^{3+} in $ZnWO_4$ crystals with an admixture in charge 5 at.% Yb + 5 at.% Li, 4 at.% Yb + 16 at.% Li and 7 at.% Tm + 24 at.% Li. The orientational behavior of the monoclinic centers Fe1, Cr1, and Gd1 in these crystals was satisfactorily described by the spin Hamiltonian (SH) with the parameters obtained in Refs. [11–16]. The triclinic centers Fe2, Fe3, Cr2, Cr3, Gd2, Gd3 disappeared or lost their intensity significantly, but new satellites (PC Fe2L, Fe3L, Cr2L, Cr3L) appeared with a different field distance from the transitions Fe1 and Cr1, which were attributed by the authors to dimer centers with the participation of Li_{Zn}. One of the Fe1 satellites turned out to be monoclinic (Fe4L) rather than triclinic. Satellite signals appeared on the wings of Gd1 centers in a limited range of angles.

Measuring the orientation behavior of the transition positions of dimeric PC (Fe2L, Fe3L, Fe4L, Cr2L, Cr3L) made it possible to obtain sets of SH parameters describing the observed angular dependencies in the optimization procedure. However, the absence of inter-doublet transitions in the spectrum raises doubts about the truth of the values obtained, as it results in a set of local minima in the optimization procedure.

2. Samples and experimental procedure

A single crystal of zinc tungstate ($ZnWO_4$) with an admixture of 4 at.% Tm + 4 at.% Li in the charge was grown by the Czochralski method. A description of charge synthesis, crystal growth, and annealing is given in Refs. [7,8,11]. This crystal was cut into four parts, from which samples suitable for EPR studies were made, named t1, t2, t3, and t4. Sample t1 is cut from the end part of the boule, sample t4 — from the beginning, and samples t2 and t3 — from the middle. All samples were rectangular parallelepipeds with polished faces (N_g, N_p, N_m) orthogonal to the axes of the optical indicatrix. It turned out that the faces of N_p and N_m in all samples are rotated around N_g by approximately 10°.

Space group $ZnWO_4$-P2/c (C_{2h}^4) No. 13, lattice cell parameters $a = 4.69$ Å, $b = 5.72$ Å, $c = 4.92$ Å, $\beta = 90.6°$ [20]. Both cations in the crystal are surrounded by six oxygen ions forming monoclinically distorted octahedra, the local symmetry group of positions Zn^{2+} and W^{6+} — 2 (C_2). The relationship of the crystallographic axes with the axes of the optical indicatrix for undoped $ZnWO_4$ is given in Refs. [5,8].

The dependence of the positions of the EPR transitions on orientation was measured when the magnetic field rotated in the **a**−**c** planes and the $N_m - \mathbf{b} \parallel Y$ axis on an EMX Plus Bruker X-band spectrometer at room temperature in magnetic fields up to 1.5 T. The parameters of the SH are given in the laboratory coordinate systems XYZ(Z ∥ of the axis N_m, Y∥ **b**), in the local coordinate system xyz of the center Cr1 (z rotated from the axis +**a** to +**c** by 4.2° [14]) and in the principal CS (PCS) of the second-rank fine structure tensor **D** (parameter $b_{20} = D$).

The sample in a spectrometer cavity was fixed to one end of a quartz tube attached to a standard automatic goniometer. To measure the angular dependencies of the EPR signal positions in the **a**−**c** plane, a 10° wedge was glued between the tube and the sample. The initial installation of the crystal in the microwave cavity (axis $N_m \parallel B$) was performed by observing the laser beam reflected from the polished face of the sample N_g through the standard window of the cavity.

The orientation behavior of the signals of monoclinic centers is well described in two planes by the SH parameters given in Ref. [11]. The angular dependences of the positions of the transitions of the Gd1 centers in the plane **a**−**c** are shown in Figure 3, where the orientation behavior of the signals detected by us in *t* samples of triclinic centers Gd2L, Gd3L (in the plane **a**−**c** two triclinic centers are equivalent). Most likely, these centers belong to dimeric associations $Gd^{3+}_{Zn^{2+}}$-$Li^{+}_{Zn^{2+}}$.

In addition, satellites (red dots) are observed on the high-field wings of the three Gd1 transitions, which have similar angular dependences to Gd1 and are probably caused by dimers Gd^{3+} with distant lithium ions. Figure 3 also shows the calculation results with parameters [11] of the angular behavior of two transitions of Gd2, Gd3 centers, attributed in Ref. [11] to dimeric associations involving zinc vacancies.

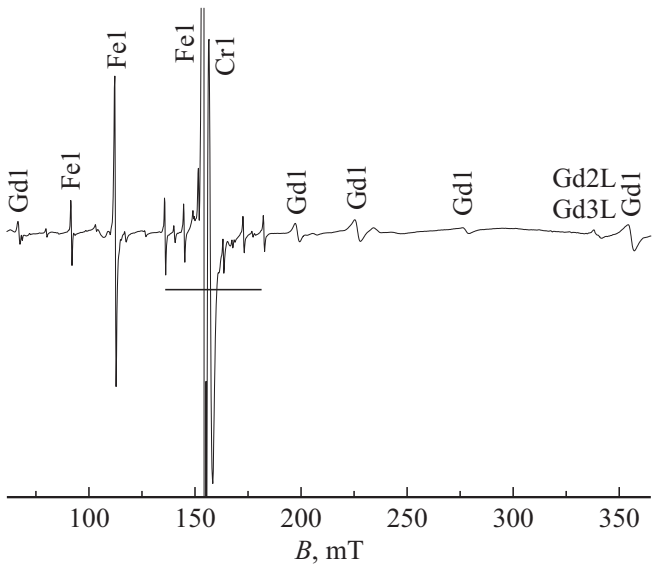

Figure 2. EPR spectrum of sample t1 at a frequency of 9576 MHz at $\theta = 90°$ in the plane **a**−**c** (see Figures 3, 5, 6). The horizontal segment indicates the position of the six components of the hyperfine Mn^{2+} structure.

It turned out that in places in all *t* samples, chains of experimental points corresponding to weak EPR signals are located along the calculated lines. Consequently, there are a small concentration of dimer centers in *t* samples $Gd^{3+}_{Zn^{2+}}$-$V_{Zn^{2+}}$ is preserved.

3. Results and discussion

Zinc tungstate crystals *t*-series doped with 4 at.% Tm + 4 at.% Li, exhibit intense EPR spectra of Fe1 and Cr1 centers, as well as weaker Gd1 (the so-called first centers) and PC Mn^{2+}, studied earlier in Refs. [11,19]. It should be noted that the spectra of the t-series are more resolved than those obtained on samples with charge doping of 5 at.% Yb + 5 at.% Li, 4 at.% Yb + 16at.% Li and 7 at.% Tm + 24 at.% Li [19], this fact is due to both a lower concentration of impurities and, apparently, the peculiarities of growing regimes. Figure 2 shows the low-field part of the spectrum of the sample t1 with intense signals Fe1, Cr1 and Gd^{3+}.

Figure 3 clearly shows that all the observed Gd^{3+} centers (one monoclinic and three triclinic) exhibit low symmetry effects, in particular, the mismatch of the positions of extrema in the angular dependences (axes) of different transitions, as well as the asymmetry of the angular dependencies [21]. These phenomena are caused by the mismatch at the low-symmetric centers of the principal axes of the fine structure tensors of the second, fourth and sixth ranks.

The results of optimizing the parameters of the SH [22] triclinic PC Gd2L, Gd3L by the least squares method using the positions of transitions in two planes are shown in

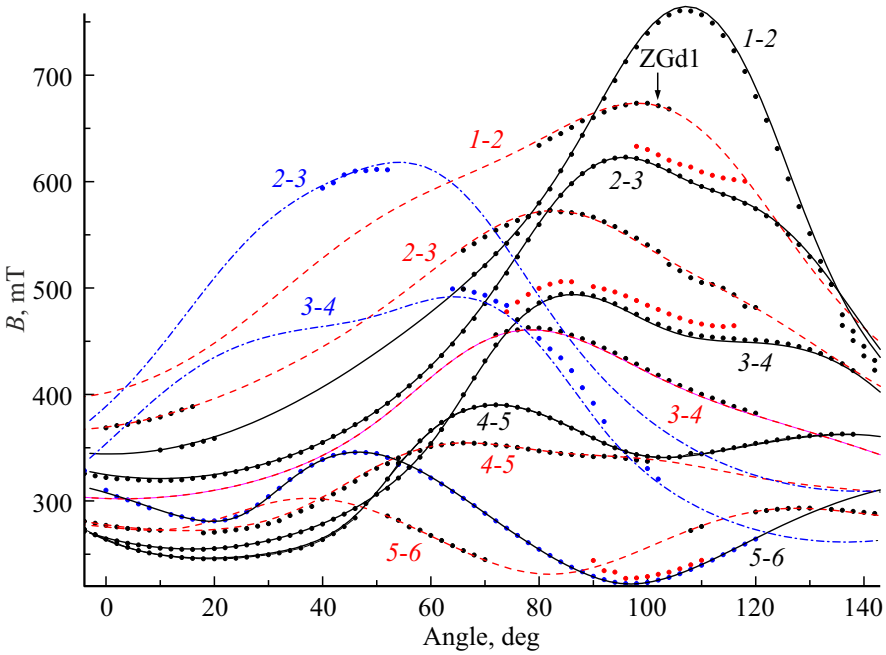

Figure 3. Angular dependences of the positions of the EPR transitions ($i-j$ -energy level numbers) of the centers Gd1 (solid black curves), Gd2L, Gd3L (dashed red), Gd2, Gd3 (dotted blue) in the plane **a**−**c** of the sample t3. Red dots — the positions of the Gd1 transition satellites. Zero of the abscissa axis — N_m.

Table 1, where the parameters of the centers Gd1 and Gd2, Gd3 from Ref. [11] are also given. The principal magnetic axis of the Gd1 monoclinic PC, taking into account the results [14] is rotated from the +**a** axis to +**c** by $\sim 73°$. The rotation of the coordinate system of the Gd2, Gd3 centers in the PCS of tensor **D** occurs sequentially around ZYZ at angles $\alpha_2 = 6.1°$, $\beta_2 = 61.3°$, $\gamma_2 = 177°$; $\alpha_3 = 173.9°$, $\beta_3 = 118.7°$, $\gamma_3 = -2.9°$, accordingly, and for the Gd2L and Gd3L centers, rotation of the tensor **D** by angles $\alpha_{2L} = 92.6°$, $\beta_{2L} = 93.6°$, $\gamma_{2L} = 175.7°$; $\alpha_{3L} = 87.4°$, $\beta_{3L} = 86.5°$, $\gamma_{3L} = -4.3°$. At the same time, as can be seen (Table 1), the fine structure tensor of the fourth rank remains off-diagonal. The parameters of the sixth rank could not be estimated due to experimental errors. There was too little experimental data to determine the SH parameters of the triclinic center represented by satellites on the wings of Gd1 transitions.

The parameters of the second-rank SH of the three gadolinium centers in the PCS of tensor **D** (according to Table 1) differ very little, which indicates a weak effect of the compensator on the amount of zero field splitting, whereas the axes of the PCS of tensor **D** are strongly rotated (so the angle between the axes z of the centers Gd2, Gd3 and Gd2L, Gd3L is $\sim 90°$).

In contrast to Refs. [11,19], there are many satellites of Fe1 PC signals in the EPR spectra of t-samples (Figures 4, 5) with similar orientation behavior (see Figure 5). Only for the outermost satellites of the first center (Fe2L, Fe3L, and Fe4L) in Figure 4, it was possible to collect experimental data sufficient to determine the parameters of

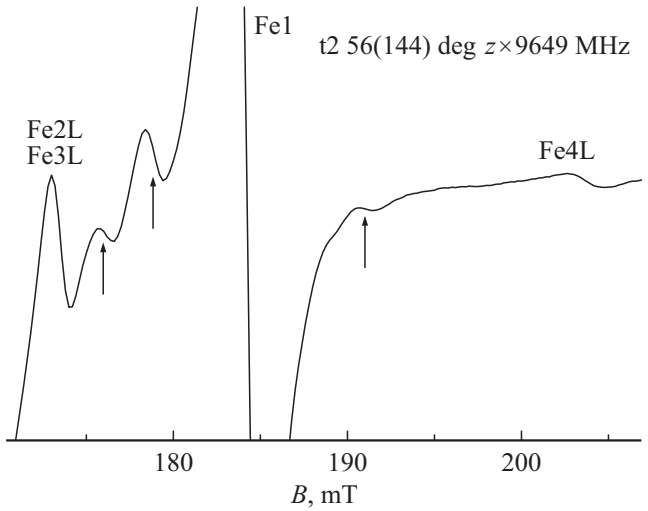

Figure 4. Fragment of the EPR spectrum of the 3−4 transition of the Fe1 center and its satellites in the sample t2 at a frequency of 9649 MHz at $\theta = 56°$ in the plane **a**−**c** (Figure 5). The arrows mark the positions of the three unexplored satellites.

their SH. The angular dependences of the positions of all intra-doublet transitions during rotation of the magnetic field in two planes were used in the procedure for optimizing the parameters of the SH of these centers.

In the case of the Fe2L and Fe3L centers, we were able to identify their high-field inter-doublet transitions 2−3 and 4−5 in both studied planes (Figures 6, 7). Figure 7 shows that the signals of the monoclinic centers Fe1 and Cr1

Table 1. Parameters* of SH of the Gd1, Gd2, Gd3 and Gd2L, Gd3L centers in different coordinate systems, $g = 1.991$. b_{nm}, c_{nm} and the standard deviation of the calculation from the experiment $F(n)$ in MHz, ZFS in GHz, (n) — number of experimental resonant values

	Gd1 PCS of tensor **D** [11]	Gd2, Gd3 Z of center Cr1 [11]	Gd2, Gd3 PCS of the tensor **D** [11]	Gd2L, Gd3L Z $\|\|$ N_m, this work	Gd2L, Gd3L PCS of tensor **D**, this work
b_{20}	1872	251	1854	202	−1773
b_{21}	0	3469	0	389	0
b_{22}	1409	2943	1400	3314	−1369
b_{40}	−1.7	−62	−19	−42	−56
b_{41}	377	9	244	273	−118
b_{42}	223	−27	−195	−77	20
b_{43}	$-1371g56$	−383	−530	537	356
b_{44}	−310	−219	−185	−249	−177
c_{21}	0	±621	0	±502	0
c_{22}	0	±566	0	±312	0
c_{41}	0	±75	−19	±119	77
c_{42}	0	±15	−75	∓19	−190
c_{43}	0	±108	−117	∓80	−64
c_{44}	0	∓137	−123	∓88	138
ZFS	$\sim 8+7+11=26$	–	$\sim 9+7+10=26$	–	$\sim 11+6+8=25$
$F(n)$	18(632)	25(450)	–	15(196)	–

* Signs b_{nm} and c_{nm} are relative.

near the plane **a**−**c** have extrema and triclinic PC Fe2L, Fe3L cease to be equivalent when moving away from the direction N_m. Entering the data obtained for Fe2L and Fe3L into the optimization procedure led to the results of Table 2.

The rotation of the coordinate system of the Fe2L, Fe3L centers in the PCS of the tensor **D** occurs sequentially around ZYZ at angles $\alpha_{2L} = 170°$, $\beta_{2L} = 50.4°$, $\gamma_{2L} = 88.6°$; $\alpha_{3L} = 10°$, $\beta_{3L} = 129.6°$, $\gamma_{3L} = -91.4°$. For the Fe4L center in the PCS of tensor **D** rotation by angles $\alpha_{4L} = 0°$, $\beta_{4L} = 130°$, $\gamma_{4L} = 270°$. As can be seen in Table 2, the SH and ZFS parameters of Fe2L, Fe3L and Fe4L centers in the PCS of tensor **D** are quite close to each other and to the parameters of Fe1: $b_{20} = -20960$ MHz, $b_{22} = 14805$ MHz, ZFS = 138 GHz, which indicates a slight disturbance of Fe^{3+} by the presence of lithium ion in its vicinity. The parameters of the SH of Fe4L center were obtained taking into account only intra-doublet transitions, but the angular dependences predicted by these parameters for the transition 4−5 fall into the region of unidentified experimental resonances (Figure 6). Most likely, more than one dimeric center is observed here (see Figure 6) with resonant fields intermediate between the dependences of Fe1 and Fe4L. By the way, there are at least five lithium PC of iron in Figures 4, 5. In this regard, it is very difficult to assign the observed (intra-doublet and inter-doublet) transitions to a specific center.

Information about the inter-doublet transition of triclinic Cr2L and Cr3L PC was obtained by measuring the EPR spectra (Figure 7) in a plane rotated around Y by +18° relative to the plane (N_m − **b** ||Y axis). These transitions are not observed in the standard plane for *t*-samples. The angle of rotation of the plane was determined by the coincidence of the positions of the resonances in two perpendicular planes under study.

Figure 8 clearly shows that there is another triclinic center Cr^{3+} (blue curves) and several monoclinic ones. The obtained angular dependences of the positions of the three Cr2L and Cr3L transitions (Figure 8), taking into account the data on intra-doublet resonances from the a-c plane, as a result of the optimization procedure, gave the SH parameters shown in Table 3 in two coordinate systems. The rotation of the CS of Cr2L, Cr3L centers in the PCS of tensor **D** occurs sequentially around ZYZ at angles $\alpha_{2L} = 141°$, $\gamma_{2L} = 20.7°$, $\beta_{2L} = 137.3°$; $\alpha_{3L} = 39°$, $\beta_{3L} = 159.3°$, $\gamma_{3L} = -43.7°$.

At the second triclinic center Cr^{3+} (blue curves in Figure 8) it was possible to obtain the angular dependencies of the positions in two planes only for the transition 2−3

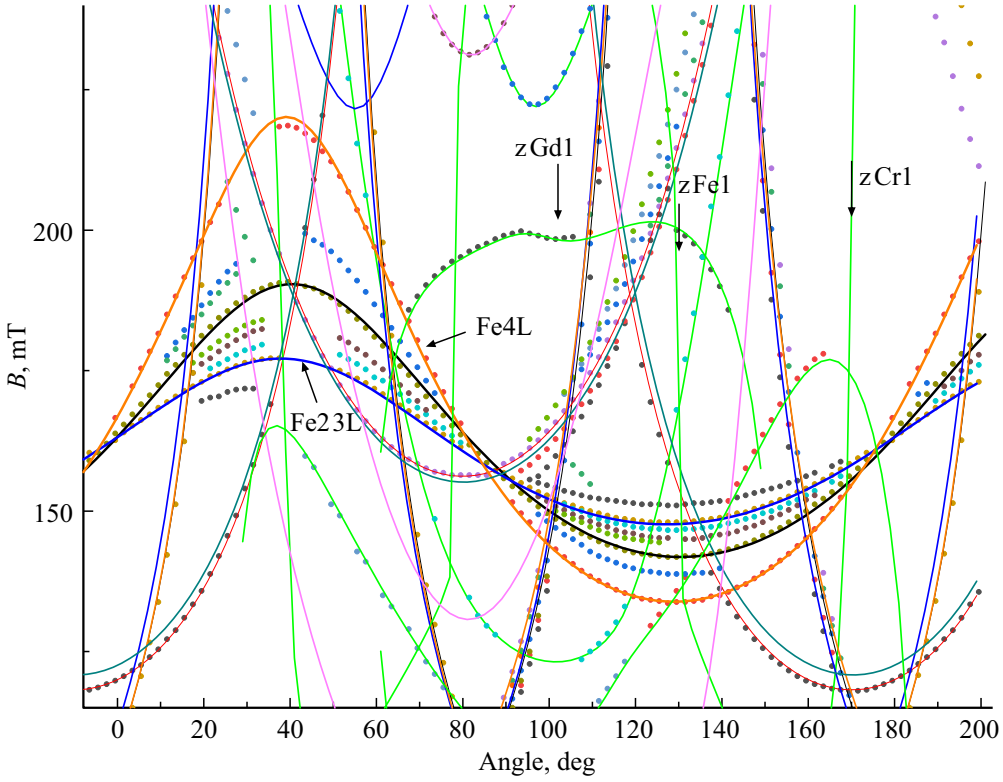

Figure 5. Orientation behavior of the 3−4 transition of the center of Fe1 and its satellites in the plane **a**−**c** at a frequency of 9649 MHz. PC Fe1 — black curves, Fe2L, Fe3L — blue, Fe4L — orange. Signals of gadolinium centers that fall into the field of the figure — green and purple curves (see Figure 3), chromium PC — red. Zero of the abscissa axis — N_m.

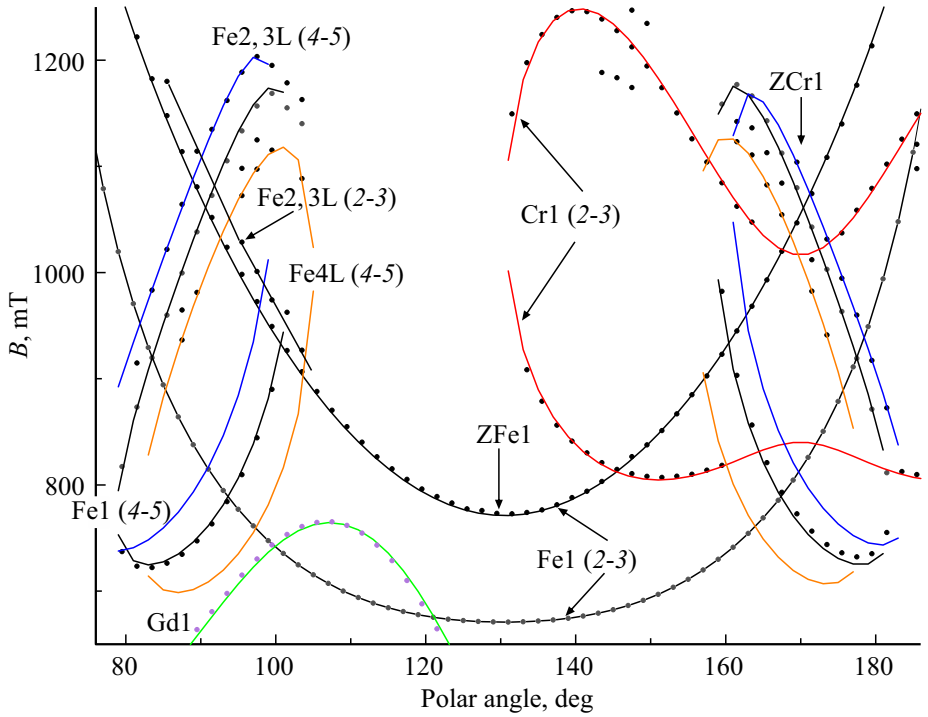

Figure 6. Fragment of the angular dependence of the positions of the transitions of the centers Fe1 (black curves), Fe2L, Fe3L (blue) and Cr1 (red) in the plane **a**−**c** at a frequency of 9649 MHz. Orange curves — dependencies of the 4−5 transition of the Fe4L center, predicted by the parameters of Table 2. Zero of the abscissa axis — N_m.

Table 2. Parameters* of SH of Fe2L, Fe3L, and Fe4L centers in t-samples, $g = 2.002$. b_{nm}, c_{nm} and $F(n)$ in MHz, ZFS in GHz, (n) — number of experimental resonance values

	Fe2L, Fe3L		Fe4L		Fe1
	Z ∥ axes N_m	PCS of tensor **D**	Z ∥ axes N_m	PCS of tensor **D**	PCS of tensor **D** [12]
b_{20}	2610	−22070	1060	−21680	−20961
b_{21}	80080	0	76120	0	0
b_{22}	−7560	−16840	−10440	−12300	14805
b_{40}	−212	−357	123	75	196
b_{41}	−530	943	243	0	0
b_{42}	−3131	−194	−148	−697	−107
b_{43}	−121	−1921	−4064	0	0
b_{44}	1399	−2242	−24	−724	−1038
c_{21}	∓15352	0	0	0	
c_{22}	±2187	0	0	0	0
c_{41}	±452	−1323	0	0	0
c_{42}	±702	−996	0	0	0
c_{43}	∓2350	8408	0	0	0
c_{44}	±523	−213	0	0	0
ZFS	64 + 81 = 145	–	57 + 82 = 139	–	61 + 77 = 138
$F(n)$	51 (308)	–	48 (230)	–	–

* Signs b_{nm} and c_{nm} are relative.

Table 3. Parameters* SH of triclinic centers Cr2L, Cr3L in *t*-samples, $g = 1.96$. b_{2m}, c_{2m} and $F(n)$ in MHz, ZFS in GHz, (n) — number of experimental resonance values

Parameters	Cr2L, Cr3L Z ∥ axes N_m, this work	Cr2L, Cr3L, PCS, this work	Cr1, PCS [11,14]
b_{20}	24590	30170	+25490
b_{21}	−50640	0	0
b_{22}	−8160	10410	−7230
c_{21}	±31550	0	0
c_{22}	∓8300	0	0
ZFS	∼ 61	–	∼ 51
$F(n)$	110(140)	–	–

* Signs b_{nm} and c_{nm} are relative.

and in a small range of angles. This turned out to be insufficient to determine reliable SH parameters.

The degree of distortion of the six-fold environment of the monoclinic centers Fe1, Cr1, and Gd1 is illustrated by the values of the parameters b_{20} and b_{22} in the principal coordinate systems (Tables 1−3, Figure 4), taking into account the fact that these parameters have zero values for PC in a cubic environment (octahedral in $ZnWO_4$). The decrease in the symmetry of dimeric PC to triclinic is reflected both in the values b_{20} and b_{22}, and in the orientation of the PCS of tensor **D**. At the same time, the change in b_{20} due to the appearance of a close compensating charge Li_{Zn} is single percent, only b_{22} changes by an amount exceeding 10 % at the Fe^{3+}, Cr^{3+} centers.

The recordings of the spectra (Figure 2) used to construct the orientation behavior of the positions of the EPR transitions (Figures 3, 5−8), do not allow a qualitative evaluation of the intensity of the observed signals. Multiple passes with extended measurement time at each point and summation

Table 4. The ratio of concentrations of lithium and vacancy gadolinium associates to the concentration of Gd1 centers in *t*-samples

	*t*1	*t*2	*t*3	*t*4
c(Gd-Li)/c(Gd1)	0.065	0.075	0.086	0.072
c(Gd-V)/c(Gd1)	0.026	0.041	0.049	0.044

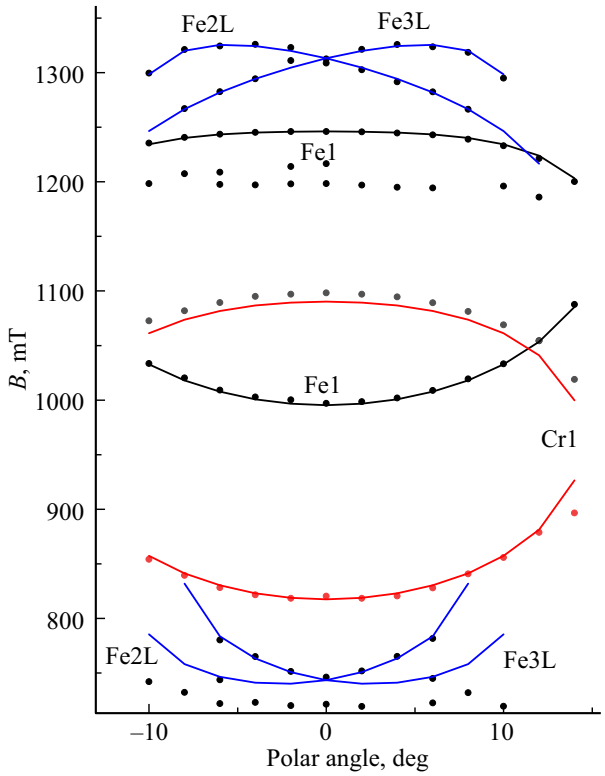

Figure 7. Angular dependence of the positions of 2−3 transitions of the centers Fe1 (black curves), Fe2L, Fe3L (blue) and Cr1 (red) in the plane of axis N_m−**b** ||Y (sample t1) at a frequency of 9571 MHz. The experimental points not identified in the figure most likely belong to the dimer centers $Fe^{3+}_{Zn^{2+}}$−$Li^{+}_{Zn^{2+}}$, the signals of some of them can be seen in Figure 4.

of the obtained spectra were performed to improve the recording quality in the magnetic field orientations $\theta = 0°$, 60° and 110° (Figures 3, 5). The spectrum of Mn^{2+} and Fe^{3+} at $\theta = 0°$ due to the small width of Mn^{2+} signals was recorded with a small amplitude (0.1 mT) of magnetic field modulation and the reduced value (0.025 mT) of the pitch step. The integral intensity was taken to be the product of the peak intensity of the first derivative of the absorption line I_{pp} per the square of the line width between the extremes of the first derivative ΔB_{pp}.

The results for gadolinium centers are shown in Table 4. As can be seen, only the ratio of concentrations c(Gd-V)/c(Gd1) noticeably ($\sim$ 1.7 times) changed in the series of samples studied, and the concentrations of dimer centers did not exceed units of %. However, in a sample with 4 at.% Tm (without lithium) in the charge, according to [11], the concentration ratio is c(Gd-V)/c(Gd1) $\approx$ 0.4. Most likely, in *t*-samples, lithium ions are mainly localized noticeably further from gadolinium than zinc vacancies, and give signals in the wings of Gd1 signals, increasing their intensity. Something similar can be seen in the Fe^{3+} spectra (Figures 4, 5), for which it was possible to measure the angular dependences of the positions only for dimeric PC signals remote from the Fe1 transitions.

The ratio of the integral intensities Mn/Fe1 in a series of t-samples with good accuracy turned out to be constant. It was noted that the integral intensity of the Fe1, Cr1, and Gd1 signals in a number of samples t1−t4, taking into account their mass, decreased by $\sim$ 30%, $\sim$ 20 % and $\sim$ 10 %, respectively.

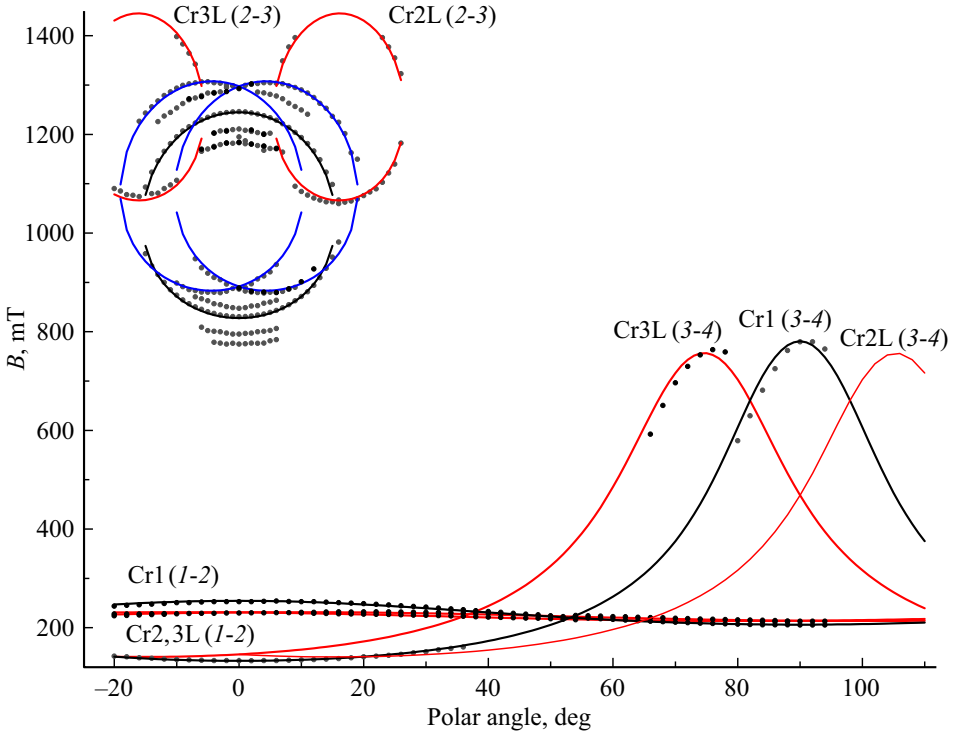

Figure 8. Orientation behavior of the EPR positions of the PC signals Cr1 (black curves), Cr2L and Cr3L (red) when the magnetic field rotates from the direction lying in the plane **a**−**c** at +18° from the axis N_m, to the **b** ||Y axis (sample t1) at a frequency of 9576 MHz.

The indicated trend in the intensity of gadolinium centers is in perfect agreement with the trend in the concentration of Tm^{3+} ions along the length of the boule, revealed by polarized optical absorption spectroscopy and given in the Introduction, according to which, from the beginning (sample t4) to the end of the boule (sample t1), the concentration of thulium also increases monotonously by about 10 %. This confirms the correctness of our approach, according to which gadolinium can be considered as a convenient marker for EPR studies of the crystallochemical behavior of other rare earth ions (including thulium) in the ZnWO crystal$_4$.

4. Conclusion

A difference was found in the behavior of the kinetics of luminescence attenuation measured at different sites of the same $ZnWO_4$ sample grown by the Czochralski method (with an admixture in the charge of 4at.% Tm + 4at.% Li). An attempt has been made using EPR to detect a correlation between the behavior of luminescence attenuation kinetics and the concentration and degree of association of uncontrolled paramagnetic impurity ions Fe^{3+}, Cr^{3+} and Gd^{3+}.

As a result of EPR studies of four t-samples from this single crystal of zinc tungstate, the transitions of triclinic Gd^{3+} PC associated with lithium ions localized in zinc positions were identified, and the parameters of their SH were determined. In addition, weak EPR signals of dimeric PC Gd^{3+}-V_{Zn} were observed in these samples. Detection of inter-doublet transitions in high fields of similar centers Fe^{3+} and Cr^{3+} with the participation of lithium ions made it possible to refine the parameters of their spin Hamiltonians and correctly determine the values of ZFS.

A change in c(Gd-V)/c(Gd1) concentration ratio and a slight decrease in the integral intensity of Fe1, Cr1, and Gd1 signals is observed across the t1–t4 sample series. It is difficult to say whether these changes are related to differences in the kinetics of luminescence attenuation in different crystal regions. This requires further research.

In particular, the studied samples of $ZnWO_4$:4at.% Tm + 4at.% Li crystal may differ in the behavior of accompanying ions Fe^{2+} or ions Tm^{3+} and their associates (both with charge compensators and with each other), which can be observed only at temperatures of liquid helium and at high microwave frequencies. It is also possible that differences between the samples will manifest themselves in the framework of measurements of the absorption and luminescence spectra of the samples at cryogenic temperatures.

Funding

The study was financially supported by the Ministry of Science and Higher Education of the Russian Federation, topic No. FEUZ-2023-0017 using the equipment provided by Ural Common Use Center „Modern Nanotechnologies“ of Ural Federal University (Reg. No. 2968).

Conflict of interest

The authors declare that they have no conflict of interest.

References

[1] V.B. Mikhailik, H. Kraus. J. Phys. D: Appl. Phys. **39**, 1181 (2006).
[2] V. Nagirnyi, E. Feldbach, L. Jonsson, M. Kirm, A. Kotlov, A. Lushchik, V.A. Nefedov, B.I. Zadneprovski. Nucl. Instrum. Methods Phys. Res. A **486**, 395 (2002).
[3] L.L. Nagornaya, A.M. Dubovik, Y.Y. Vostretsov, B.V. Grinyov, F.A. Danevich, K.A. Katrunov, V.M. Mokina, G.M. Onishchenko, D.V. Poda, N.G. Starzhinskiy, I.A. Tupitsyna. IEEE Trans. Nucl. Sci. **55**, *3*, 1469 (2008).
[4] P.A. Popov, S.A. Skrobov, A.V. Matovnikov, N.V. Mitroshenkov, V.N. Shlegel, Yu.A. Borovlev. Phys. Solid State **58**, *4*, 853 (2016).
[5] Gh.Z. Elabedine, K. Subbotin, P. Loiko, Z. Pan, K. Eremeev, Y. Zimina, Y. Didenko, S. Pavlov, A. Titov, E. Dunina, L. Fomicheva, A. Kornienko, A. Braud, R.M. Solé, M. Aguiló, F. D'ıaz, W. Chen, P. Volkov, V. Petrov, X. Mateos. Opt. Mater. **157**, 116039 (2024).
[6] Yu.I. Zimina, K.A. Subbotin, A.I. Titov, P.A. Volkov, Ya.S. Didenko, D.A. Lis, S.K. Pavlov, E.V. Zharikov. Phys. Wave Phenom. **33**, 227 (2025).
[7] K.A. Subbotin, A.I. Titov, S.K. Pavlov, P.A. Volkov, V.V. Sanina, D.A. Lis, O.N. Lis, Y.I. Zimina, Y.S. Didenko, E.V. Zharikov. J. Cryst. Growth **582**, 126498 (2022).
[8] A. Volokitina, S.P. David, P. Loiko, K. Subbotin, A. Titov, D. Lis, R.M. Sole, V. Jambunathan, A. Lucianetti, T. Mocek, P. Camy, W. Chen, U. Griebner, V. Petrov, M. Aguilo, F. D'ıaz, X. Mateos. J. Lumin. **231**, *231*, 117811 (2021).
[9] M. Buryi, V.V. Laguta, J. Hybler, M. Nikl. Phys. Status Solidi B **248**, 993 (2011).
[10] E.N. Galashov, V.A. Gusev, V.N. Shlegel, Ya.V. Vasiliev. Crystallography Reports **54**, *4*, 689 (2009).
[11] V.A. Vazhenin, A.P. Potapov, K.A. Subbotin, M.Yu. Artemov, Yu.I. Zimina, A.V. Fokin, A.I. Titov, D.A. Lis, P.A. Volkov. FTT **67**, 478 (2025) (in Russian).
[12] W.G. Nilsen, S.K. Kurtz. Phys. Rev. **136**, A262 (1964).
[13] A.A. Galkin, G.N. Neilo, G.A. Tsintsadze. FTT **9**, 359 (1967) (in Russian).
[14] S.K. Kurtz, W.G. Nilsen. Phys. Rev. **128**, 1586 (1962).
[15] E.N. Emel'yanova, N.V. Karlov, A.A. Manenkov, V.A. Milyaev, A.M. Prokhorov, S.P. Smirnov, A.V. Shirkov. ZhETF **44**, 868 (1963) (in Russian).
[16] A.A. Ryadun, E.N. Galashov, V.A. Nadolinnyi, V.N. Shlegel'. Zhurnal strukturnoi chimii **53**, 696 (2012) (in Russian).
[17] A. Watterich, M. Wöhlecke, H. Müller, K. Raksanyij, A. Breitkopf, B. Zelei. J. Phys. Chem. Solids **53**, 889 (1992).
[18] V.A. Atsarkin, L.P. Litovkina, M.L. Meil'man. FTT **7**, 3099 (1965) (in Russian).
[19] V.A. Vazhenin, M.Yu. Artemov, A.P. Potapov, K.A. Subbotin, A.V. Fokin, Yu.I. Zimina, A.I. Titov, D.A. Lis. FTT **67**, 1654 (2025) (in Russian).
[20] W.S. Brower Jr., P.H. Fang. J. Appl. Phys. **41**, 2266 (1970).
[21] M.L. Meilman, M.I. Samoilovich. Vvedeniye v spektroskopiyu EPR aktivirovannykh monokristallov. Atomizdat, M. (1977). p. 270 (in Russian).
[22] S.A. Al'tshuler, B.M. Kozyrev. Elektronnyi paramagnitnyi rezonans soedinenii elementov promezhutochnykh grupp. Nauka, M. (1972). p. 121 (in Russian).

Translated by A.Akhtyamov